Analysis of galaxy kinematics based on Cepheids from the Gaia DR2 Catalogue

V. V. Bobylev,[1]★ A. T. Bajkova,[1] A. S. Rastorguev[2,3] and M. V. Zabolotskikh[2]

[1]*Central (Pulkovo) Astronomical Observatory of RAS, 65/1 Pulkovskoye Chaussee, Saint Petersburg 196140, Russia*
[2]*Sternberg Astronomical Institute, Lomonosov Moscow State University, 13 Universitetskii prospest, Moscow 119992, Russia*
[3]*Faculty of Physics, Lomonosov Moscow State University, 1 bldg. 2, Leninskie Gory, Moscow 119991, Russia*

ABSTRACT

To construct the rotation curve of the Galaxy, classical Cepheids with proper motions, parallaxes and line-of-sight velocities from the Gaia DR2 Catalogue are used in large part. Our working sample formed from literature data contains about 800 Cepheids with estimates of their age. We determined that the linear rotation velocity of the Galaxy at the solar distance is $V_0 = 240 \pm 3$ km s^{-1}. In this case, the distance from the Sun to the axis of rotation of the Galaxy is found to be $R_0 = 8.27 \pm 0.10$ kpc. A spectral analysis of radial and residual tangential velocities of Cepheids younger than 120 Myr showed close estimates of the parameters of the spiral density wave obtained from data both at the present time and in the past. Therefore, the value of the wavelength $\lambda_{R,\theta}$ is in the range [2.4–3.0] kpc, the pitch angle $i_{R,\theta}$ is in the range [$-13°, -10°$] for a four-arm pattern model, and the amplitudes of the radial and tangential perturbations are $f_R \sim 12$ km s^{-1} and $f_\theta \sim 9$ km s^{-1}, respectively. Velocities of Cepheids older than 120 Myr currently give a wavelength $\lambda_{R,\theta} \sim 5$ kpc. This value differs significantly from the one we obtained from samples of young Cepheids. An analysis of the positions and velocities of old Cepheids, calculated by integrating their orbits backward in time, made it possible to determine significantly more reliable values of the parameters of the spiral density wave: wavelength $\lambda_{R,\theta} = 2.7$ kpc and amplitudes of radial and tangential perturbations $f_R = 7.9$ km s^{-1} and $f_\theta = 5$ km s^{-1}, respectively.

Key words: stars: distances – variables: Cepheids – Galaxy: kinematics and dynamics – galaxies: general – galaxies: spiral.

1 INTRODUCTION

Cepheids are of great interest because they implement an independent scale of astronomical distance. For these variable stars, this is possible thanks to the period–luminosity relation (PLR: Leavitt 1908; Leavitt & Pickering 1912) and period–Wesenheit relation (Madore 1982; Caputo, Marconi & Musella 2000). Currently, these relations are well calibrated using high-precision trigonometric parallaxes of stars (Ripepi et al. 2019). The use of these relations allows us to estimate the distances to Cepheids with random errors smaller than 10 per cent (Berdnikov, Dambis & Vozyakova 2000; Sandage & Tamman 2006; Skowron et al. 2019). Note that Lazovik & Rastorguev (2020) derived the PLR by a new method, using multiphase temperature measurements, which made it possible to calculate the most accurate individual colour excesses of Cepheids. This method is based on the Baade–Becker–Wesselink approach, and in practise does not use trigonometric parallaxes.

Classical Cepheids are young (under ∼400 million years old) supergiant stars with periods of radial pulsations from ∼1 to ∼100 days. They are attributed to the flat component of the stellar population of the Galaxy, therefore they are used to study the structural and kinematic features of the Galactic disc.

In the works of various authors (Joy 1939; Pont et al. 1997; Metzger et al. 1998), the rotation parameters of the Galaxy were determined using only the distances and line-of-sight velocities of Cepheids.

To determine the Galactic rotation parameters, the combination of distances, line-of-sight velocities, and proper motions of Cepheids was used, for example, in Frink, Fuchs & Wielen (1995). In this case, proper motions were taken from the Positions and Proper Motions (PPM: Röser & Bastian 1988) catalogue, which is not very accurate.

On the basis of classical Cepheids with proper motions from the *Hipparcos* Catalogue (Hipparcos 1997), the Galactic rotation parameters (Feast & Whitelock 1997; Mel'nik et al. 2015), parameters of the spiral structure (Mel'nik et al. 1999; Bobylev & Bajkova 2012; Dambis et al. 2015), and parameters of Galactic disc flexure (Bobylev 2013a,b) were refined. Based on Cepheids of type II (the old, low-mass counterparts to classical Cepheids), the parameters of the central bulge and the distance to the Galactic Centre (Majaess, Turner & Lane 2009) were determined.

The measurements obtained by the space experiment *Gaia* (Prusti et al. 2016) are unprecedented in accuracy and volume for the study of our Galaxy. Currently the second version of the catalogue, Gaia DR2, has been published (Brown et al. 2018). The average errors of trigonometric parallaxes of bright stars ($G < 15$ mag) in this catalogue lie in the range 0.02–0.04 milliarcseconds (mas), and for faint stars ($G = 20$ mag) they are of the order of 0.7 mas. Similarly, the proper-motion errors vary from 0.05 mas year^{-1} for bright ($G < 15$ mag) to 1.2 mas year^{-1} for faint ($G = 20$ mag) stars. Line-of-sight velocities of more than 7 million stars are measured. For stars of spectral classes F–G–K, the average error of the line-of-sight velocities is about 1 km s^{-1}.

★ E-mail: vbobylev@gao.spb.ru

The problem of establishing the zero-point of parallaxes in the Gaia DR2 Catalogue is known. Already Lindegren et al. (2018) has indicated the presence of a possible systematic parallax zero-point offset of $\Delta\pi = -0.029$ mas in Gaia DR2 relative to the inertial reference frame. Currently, there are several reliable independent estimates of this offset. From a comparison of eclipsing binary stars, Stassun & Torres (2018) found $\Delta\pi = -0.082 \pm 0.033$ mas. This value is confirmed by other authors: in particular, in the analysis of Cepheids, $\Delta\pi = -0.046 \pm 0.013$ mas (Riess et al. 2018a), $\Delta\pi = -0.049 \pm 0.018$ mas (Groenewegen 2018), $\Delta\pi = -0.071 \pm 0.038$ mas (Skowron et al. 2019), and asteroseismology, $\Delta\pi = -0.053 \pm 0.009$ mas (Zinn et al. 2019). Period-luminosity-metallicyty relation were derived by a hierarchical Bayesian approach for approximately 400 RR Lyrae stars with optical and near-infrared (NIR) photometry and Gaia DR2 data (Muraveva et al. 2019) to give $\Delta\pi \approx -(0.54-0.62)$ mas. Note that the work of Riess et al. (2018a) used 50 long-period Cepheids with high-precision photometry performed with the *Hubble Space Telescope*. In the work of Groenewegen (2018), a sample of 452 classical Cepheids was used and 251 classical Cepheids were used in the work of Skowron et al. (2019).

Skowron et al. (2019) built a three-dimensional map of the distribution of 2431 Cepheids in the Galaxy. For this, the classical Cepheids of the main Optical Gravitational Lensing Experiment (OGLE: Udalski, Kubiak & Szymański 1997) were supplemented by Cepheids from the General Catalogue of Variable Stars (GCVS: Samus' et al. 2017), All Sky Automated Survey (ASAS: Pojmański 2002), and about 200 Cepheids from the Gaia DR2 Catalogue and a number of other sources. Using such a large sample, these authors specified the parameters of the density distribution of Galactic Cepheids using an exponential law and the parameters of the warped galactic disc. We note their figs 3 and 4, from which it is seen how young Cepheids trace a galactic spiral pattern.

In the work of Mróz et al. (2019), performed using 773 classical Cepheids with proper motions and line-of-sight velocities from the Gaia DR2 Catalogue, the Galactic rotation parameters were determined with the highest accuracy. In particular, the Galactic rotation velocity at a solar distance was found to be $V_0 = 233.6 \pm 2.8$ km s^{-1}, and its first derivative $V_0' = -1.34 \pm 0.21$ km s^{-1} kpc^{-1}. As shown by Bobylev & Bajkova (2012), some of the spiral density-wave parameters depend on the age of Cepheids: for example, the phase of the Sun in a spiral wave. Therefore, it is interesting to determine such parameters using Cepheids of different ages from the latest data.

When analysing maser sources, Rastorguev et al. (2017) obtained the rotation curve parameters in combination with the Strömberg asymmetry parameters, which allowed us to estimate the exponential scale of the Galactic disc under the assumption of marginal stability of the intermediate-age disc. It is interesting to compare the results of this approach in application to the kinematics and position data of a large sample of Cepheids.

In the work of Gnaciński (2019), it has been shown that the rotation velocities of classical Cepheids, obtained in three ways, (1) only from line-of-sight velocities, (2) only from proper motion (Gaia DR2), and (3) from full three-dimensional velocity vectors, are located between flat and Keplerian rotation curves. Using a large sample of Cepheids, Ablimit et al. (2020) estimated the rotation velocity of the Galaxy at the Sun's position and found the virial mass of the Galaxy and local dark matter density.

Using a large number of stars from Gaia DR2, Kawata et al. (2018) have generated maps of the rotation velocity, V_{circ}, and vertical velocity, V_z, distributions as a function of the Galactocentric radius, R. In the $R - V_z$ distribution, they found that the peak of the V_z distribution shows wave-like features.

Cepheids, as unique 'standard candles', play an important role in the construction of a universal distance scale, due to the presence of period–luminosity relations. These high-luminosity stars can be detected and studied with large ground-based and space telescopes in disc galaxies up to distances of 20–30 Mpc. Cepheid distances in up to several tens of galaxies, where supernova explosions of type Ia were recorded, have long served as the basis for calibrating the luminosities of these supernovae at their maximum brightness. As a consequence, Hubble diagrams for type Ia cosmological supernovae led to the discovery of the accelerated expansion of the Universe ('dark energy': see Riess et al. 1998, 2004; Perlmutter et al. 1997, 1999; Schmidt et al. 1998, and others).

The combined use of Hubble diagrams for type Ia cosmological supernovae, data on the cosmic microwave background (CMB) anisotropy measured by the *Wilkinson Microwave Anisotropy Probe* (*WMAP*) and *Planck* space missions, and the results of study of the large-scale distribution of galaxies (barionic acoustic oscillations: BAO) has made it possible to set restrictions on the values of global cosmological parameters: the contribution of baryonic and non-baryonic matter and that of dark energy to the total mass–energy density, as well as the curvature parameter and the equation of state (see the most important recent articles by Betoule et al. 2014; Abbott et al. 2019; Scolnic et al. 2018).

In the last 5–6 years, strong evidence has appeared in favour of a significant discrepancy between the values of the Hubble constant H_0 determined from the CMB anisotropy and from the redshifts of galaxies and the brightest optical 'standard candles' – Type Ia supernovae, the luminosities of which are based on the Cepheid distances of galaxies. Cepheid methods lead to systematically higher H_0 values by about 6–7 km s^{-1} Mpc^{-1} at a significance level of more than 4σ. This problem is now well known as 'Hubble tension' (see, for example, Riess et al. 2018b, 2020; Verde et al. 2019, and references therein).

Note that the group of CMB-based estimates is often referred to as 'global', referring to the early Universe, while the Cepheid-based group is called 'local', referring to the recent-epoch Universe. The reasons for the differences and ways of solving the 'tension' problem are being actively discussed (for example, we found about 750 articles with mention of the term 'Hubble tension' in the abstracts of articles published during last 5 years). In most works, the problem of Hubble tension is analysed from a theoretical point of view concerning the properties of dark energy and the refinement of existing models of the Universe.

However, it is possible that the reason for Hubble tension can be partly explained by the existence of some systematic errors in the Cepheid distance scales used, though the random relative errors of Cepheid distances are within 10 per cent. The main reason for possible systematics is commonly attributed to the differences in the metallicity of galaxies hosting Cepheids. Sandage & Tamman (2006) discussed this issue in detail, but the question is still the topic of numerous debates. The second reason is the systematic errors of different kinds that arise during calibration of the PLR by trigonometric parallaxes: some are due to non-linear conversion of parallaxes to distances, and some to parallax zero-point offset inherent in the Gaia DR2/EDR3 catalogues, discovered in a large number of studies (see the discussion above). The PLRs derived by the Baade–Wesselink technique can also be distorted by systematic errors. An additional source of possible errors in Hubble constant determinations based on the redshifts of galaxies and supernova stars is an underestimation of the influence of the velocity dispersion of
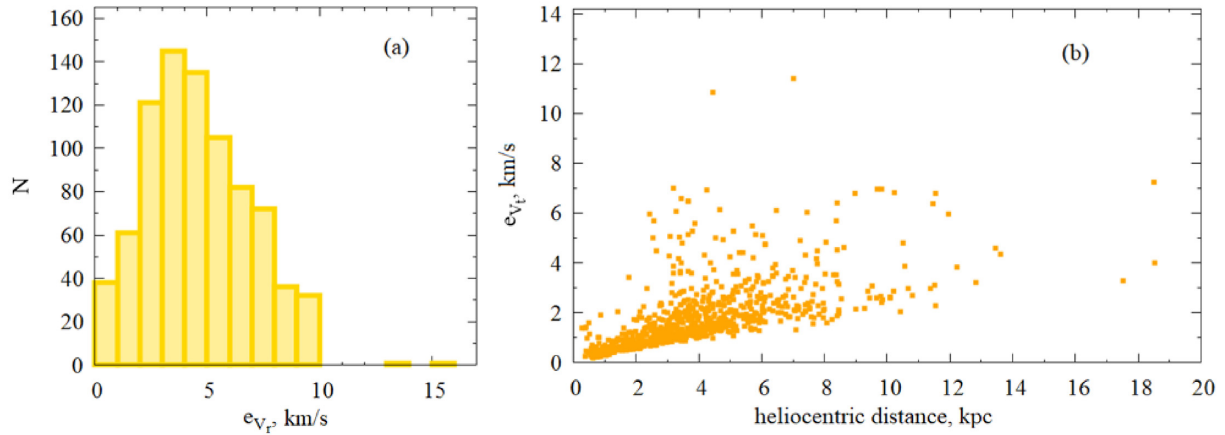
Figure 1. (a) A histogram of random errors of line-of-sight velocities of Cepheids and (b) errors of the tangential velocities of these stars versus heliocentric distance.

galaxies in galaxy clusters (see, for example, Sedgwick et al. 2021). All these issues affecting the accuracy of the distance scale, including systematic effects, are discussed in the literature, but, for the detailed analysis of the kinematics of Galactic Cepheids presented in this article, they do not constitute a serious problem.

The aim of this work is to estimate the rotation parameters of the Galaxy, as well as spiral density-wave parameters, using a large sample of classical Cepheids of different ages with proper motions and line-of-sight velocities taken from the Gaia DR2 Catalogue.

2 DATA

In this work, we use the data on classical Cepheids from the works of Mróz et al. (2019) and Skowron et al. (2019).

The catalogue of Skowron et al. (2019) contains distance, age, pulsation period, and mid-infrared (mid-IR) data from the *Spitzer* (Benjamin et al. 2003; Churchwell et al. 2009) and *WISE* space telescopes (Wright et al. 2010; Mainzer et al. 2011) for 2431 Cepheids. The distances to these stars, r, were calculated by Skowron et al. (2019) on the base of the MIR PLR of Wang et al. (2018) and mid-infrared light curves, where the influence of interstellar absorption is much smaller than in the optical.

There is a debate concerning period–age relations (Turner 2012). Several known calibrations are proposed to estimate the mean age of Cepheids: for example, the theoretical calibration performed by Bono et al. (2005) and the calibration by Efremov (2003), obtained by analysis of Cepheids in the Large Magellanic Cloud. To estimate the age of Cepheids, Skowron et al. (2019) used the calibration from the work of Anderson et al. (2016).

We note that a fundamental property of stars such as rotation (Anderson et al. 2016) is of great importance for the study of classical Cepheid variable stars. The models by Anderson et al. (2016) include rotation, while some other stellar models (Bono et al. 2005) do not, which makes the Cepheids 1.5–2 times younger. It should also be noted that the ages derived by Skowron et al. (2019) were extrapolated from Anderson et al. (2016) for metal-rich Cepheids.

The catalogue of Mróz et al. (2019) contains data on 832 classical Cepheids. The proper motions and line-of-sight velocities of stars included in the catalogue, with appropriate errors, are taken from the Gaia DR2 Catalogue. We supplemented the catalogue of Mróz et al. (2019) with estimates of the age of Cepheids from the work of Skowron et al. (2019).

Heliocentric distances to Cepheids were taken from columns 76–81 of the catalogue of Mróz et al. (2019). These, in turn, are taken from the work of Skowron et al. (2019), where they were calculated using the MIR PLR of Wang et al. (2018) and mid-infrared light curves, which remove the effects of interstellar extinction virtually.

Apparent stellar magnitudes of Cepheids observed in the OGLE programme lie in the range $I = 11$–18 mag (Skowron et al. 2019). Therefore, in the Mróz et al. (2019) and Skowron et al. (2019) catalogues there is a deficiency of bright and well-studied Cepheids from earlier observations.

According to Skowron et al. (2019), the errors in distances to Cepheids are ~5 per cent. The problem is that there may be systematics at play toward certain directions, and at given short and long Galactocentric radii, where metallicity and R (ratio of total-to-selective extinction) differences may also be at play.

Random line-of-sight velocity errors e_{V_r} usually do not exceed 10 km s^{-1}; on average they are 5 km s^{-1}. A typical proper-motion error of about 0.1 mas year^{-1} will give a tangential velocity error $e_{V_t} = 5$ km s^{-1} ($0.1 \times 4.741 \times r$) only for heliocentric distances greater than 10 kpc. Thus, in our sample, random line-of-sight velocity errors introduce the main contribution to random errors of spatial velocities.

The errors in distances and line-of-sight velocities have been taken from the catalogue of Mróz et al. (2019). Fig. 1 represents a histogram of random line-of-sight velocity errors e_{V_r} of Cepheids (left-hand panel) and errors of tangential velocities e_{V_t} of these stars versus heliocentric distance (right-hand panel). It can be seen from the figure that our approximate estimate is in good agreement with the actual distribution of Cepheid random velocity errors.

3 METHOD

3.1 Galaxy rotation curve parameters

We use a rectangular coordinate system centred on the Sun. The x-axis is directed towards the Galactic Centre, the direction of the y-axis coincides with the direction of rotation of the Galaxy, and the z-axis is directed towards the North Pole of the Galaxy. Then the rectangular coordinates are calculated as follows: $x = r \cos l \cos b$, $y = r \sin l \cos b$ and $z = r \sin b$. This coordinate system is shown in Fig. 2(c).
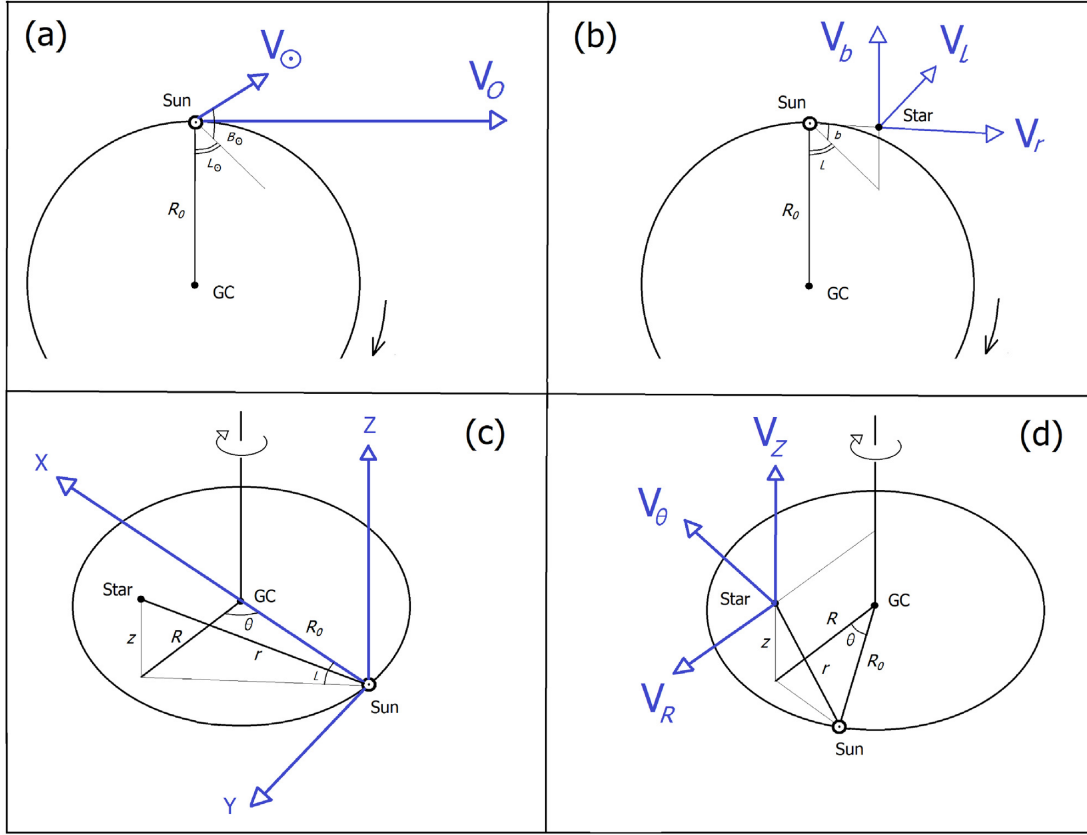
Figure 2. (a) The peculiar velocity of the Sun $V_\odot$ and circular rotational velocity of the Sun V_0 around the Galactic Centre (GC) at distance R_0, (b)the velocity components V_r, V_l, and V_b, (c) coordinate system x, y, and z, and (d) cylindrical coordinate system V_R, V_θ, and V, where thin black arrows indicate the direction of rotation of the Galaxy.

Astrometric observations give three components of stellar velocity: the line-of-sight velocity V_r and two projections of the tangential velocity: $V_l = 4.74\,r\,\mu_l \cos b$ and $V_b = 4.74\,r\,\mu_b$, directed along the Galactic longitude l and latitude b, respectively. All the velocity components are measured in km s^{-1}. Proper motion components $\mu_l \cos b$ and μ_b are determined in mas year^{-1}. The coefficient 4.741 is equal to the ratio of the number of km in an astronomical unit to the number of seconds in a tropical year, and r is the star's heliocentric distance in kpc. The velocities V_r, V_l, and V_b are shown in Fig. 2(b).

For stars with known line-of-sight velocities, proper motions, and distances, the spatial velocities U, V, W are calculated as follows:

$$U = V_r \cos l \cos b - V_l \sin l - V_b \cos l \sin b,$$

$$V = V_r \sin l \cos b + V_l \cos l - V_b \sin l \sin b,$$

$$W = V_r \sin b + V_b \cos b. \tag{1}$$

Herewith the velocity U is directed from the Sun to the Galactic Centre, V is in the direction of Galactic rotation and W is directed towards the North Galactic Pole.

In further studies of the galactic spiral density wave, we also use the following two very important velocities: the radial velocity V_R, directed from the centre of the Galaxy to the star, and the tangential velocity $V_{\rm circ}$, orthogonal to V_R and directed towards the rotation of the Galaxy, which are calculated using the following formulae:

$$V_{\rm circ} = U \sin \theta + (V_0 + V) \cos \theta,$$

$$V_R = -U \cos \theta + (V_0 + V) \sin \theta, \tag{2}$$

where R_0 is the galactocentric distance of the Sun, V_0 is the linear circular rotation velocity around the Galactic Centre in the solar neighbourhood, R is the distance from the star to the axis of Galactic rotation,

$$R^2 = r^2 \cos^2 b - 2R_0 r \cos b \cos l + R_0^2, \tag{3}$$

and the position angle θ follows the relation $\tan \theta = y/(R_0 - x)$. Components V_R, V_θ (in our case $V_\theta \equiv V_{\rm circ}$) and V_z are shown in Fig. 2(d).

We determine the parameters of the Galactic rotation curve by solving equations based on Bottlinger's formulae, in which the angular velocity Ω is expanded into a Taylor series in powers of $(R - R_0)$ to terms of the i-th order of smallness of r/R_0:

$$V_r = -U_\odot \cos b \cos l - V_\odot \cos b \sin l - W_\odot \sin b$$
$$+ R_0 \sin l \cos b \left[\sum_{i=1}^{N} (R - R_0)^i \frac{\Omega_0^{(i)}}{i!} \right], \tag{4}$$

$$V_l = U_\odot \sin l - V_\odot \cos l - r\Omega_0 \cos b$$
$$+ (R_0 \cos l - r \cos b) \left[\sum_{i=1}^{N} (R - R_0)^i \frac{\Omega_0^{(i)}}{i!} \right], \tag{5}$$

$$V_b = U_\odot \cos l \sin b + V_\odot \sin l \sin b - W_\odot \cos b$$
$$- R_0 \sin l \sin b \left[\sum_{i=1}^{N} (R - R_0)^i \frac{\Omega_0^{(i)}}{i!} \right]. \tag{6}$$
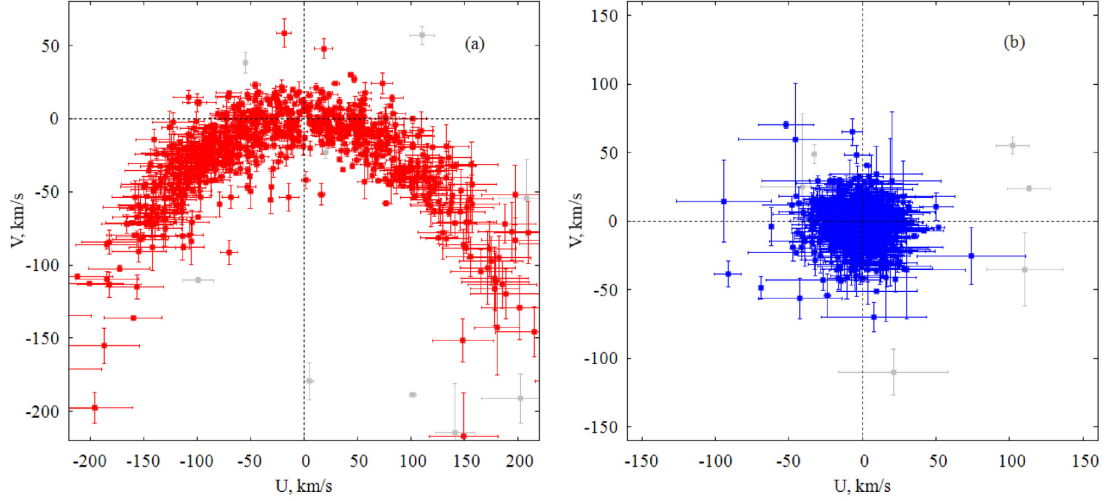
Figure 3. Cepheid U, V velocities: (a) uncorrected and (b) corrected for the differential Galactic rotation; grey symbols indicate stars that were discarded according to the restrictions (10).

The values $U_\odot$, $V_\odot$, and $W_\odot$ are group velocities, which contain the peculiar motion of the Sun (see Fig. 2a) and the contribution from the effect called 'asymmetric drift', which is considered to be small in the case of Cepheids and other young populations. The value Ω_0 is the angular velocity of the Galaxy at a solar distance R_0, $\Omega_0^{(i)}$ is the ith derivative of the angular velocity with respect to R, and the linear rotation velocity at the solar distance equals $V_0 = R_0\Omega_0$. In the coordinate system x, y, z shown in Fig. 2(c) with positive rotation around the z-axis, there will be rotation from the x-axis to the y-axis. In this case, the sign of the angular velocity Ω will be negative, which is not always convenient. We prefer to have a positive Ω. Therefore, equations (4)–(6) are written appropriately (such a coordinate system is shown later).

3.2 Residual velocity formation

The residual velocities are calculated taking into account the peculiar motion of the Sun, $U_\odot$, $V_\odot$, and $W_\odot$ (see Fig. 2a), as well as the influence of the differential rotation of the Galaxy, in the following way:

$$V_r = V_r^* - \left[- U_\odot \cos b \cos l - V_\odot \cos b \sin l - W_\odot \sin b \right.$$
$$+ R_0(R - R_0) \sin l \cos b \Omega_0'$$
$$\left. + 0.5 R_0(R - R_0)^2 \sin l \cos b \Omega_0'' + \dots \right], \quad (7)$$

$$V_l = V_l^* - \left[U_\odot \sin l - V_\odot \cos l - r\Omega_0 \cos b \right.$$
$$+ (R - R_0)(R_0 \cos l - r \cos b)\Omega_0'$$
$$\left. + 0.5(R - R_0)^2(R_0 \cos l - r \cos b)\Omega_0'' + \dots \right], \quad (8)$$

$$V_b = V_b^* - \left[U_\odot \cos l \sin b + V_\odot \sin l \sin b - W_\odot \cos b \right.$$
$$- R_0(R - R_0) \sin l \sin b \Omega_0'$$
$$\left. - 0.5 R_0(R - R_0)^2 \sin l \sin b \Omega_0'' - \dots \right], \quad (9)$$

where V_r^*, V_l^*, V_b^* on the right-hand sides of the equations are the initial velocities, and on the left-hand sides are the corrected velocities V_r, V_l, V_b, which can be used for calculation of the residual velocities U, V, W by formulae (1).

The original spatial velocities of stars usually contain a small percentage of values that differ significantly from the average. Such velocities should be discarded using some criterion. Fig. 3 shows the Cepheid U, V velocities calculated using relations (1). All Cepheids (820 stars) were used to build this picture, without any preliminary rejection. We see that, before analysing such velocities in order to detect rebounds, they must be corrected for the differential rotation of the Galaxy.

Note that the application of the rotation curve obtained on the basis of equations (4)–(6) has a restriction on R (Fig. 4). Therefore, for purposes such as detecting bounces when analysing the residual tangential velocities $|\Delta V_{\text{circ}}|$, we can simply use the flat rotation curve, $V_{\text{circ}} = const$. The velocities W and V_R do not depend on the rotation curve of the Galaxy (see equation 2). As a result, to remove bounces from the sample, we apply the following restrictions:

$$|V_R| < 90 \text{ km s}^{-1},$$
$$|\Delta V_{\text{circ}}| < 90 \text{ km s}^{-1},$$
$$|W| < 60 \text{ km s}^{-1}. \quad (10)$$

Note that the criteria (10) are only used for a preliminary cleaning of the sample, while another rejection criterion (velocity residuals in excess of 3σ) will be applied in the analysis.

It is known that the movement of gas and young stars is influenced by the central Galactic bar (Chemin, Renaud & Soubiran 2019). Some authors refer to the bar as a structure with a half-length of 2.5 kpc with a position angle of 15–30° with respect to the Sun–Galactic Centre direction (Babusiaux & Gilmore 2005; Lopez-Corredoira, Cabrera-Lavers & Gerhard 2005), while other researchers suggest that there is a long massive bar with a half-length of 4–5 kpc and a position angle of around 45° (Hammersley et al. 1994; Wegg, Gerhard & Portail 2015). Moreover, according to some authors (Alard 2001; Nishiyama et al. 2005), there is also a very small inner bar embedded in the very central bar/bulge structure with a different orientation compared with the other two bars.

The strongest influence (deviations from the flat rotation curve of more than ~50 km s^{-1}, an increase in velocity dispersions) on the velocity of objects due to the bar is observed in the region of 1.5–2 kpc (Clemens 1985; Bhattacharjee, Chaudhury & Kundu 2014; Bajkova & Bobylev 2016), while a weak gravitational influence can
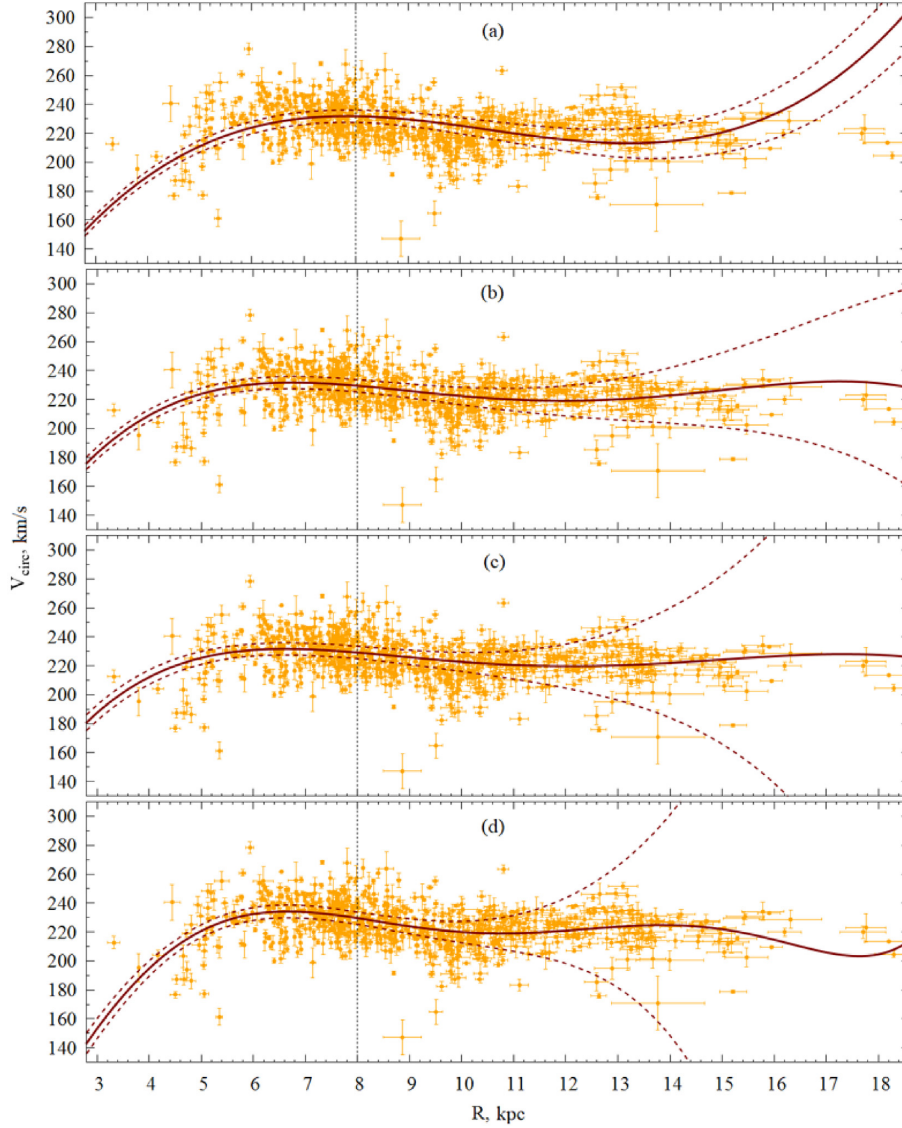
Figure 4. The rotation velocities of Cepheids V_{circ} versus the distance R, the galaxy rotation curve found from these stars with (a) two, (b) three, (c) four, and (d) five derivatives of the angular velocity of rotation; for each curve, the confidence interval limits corresponding to the error level of 1σ are marked with dashed lines; all curves are calculated for the accepted value of $R_0 = 8$ kpc. The vertical line marks the position of the Sun.

be traced up to 5 kpc (Chemin et al. 2019). To exclude the influence of the bar, it is advisable to apply the restriction $R > 2.5$ kpc as an initial condition. As can be seen from Figs 4 and 5, in practise, almost all the Cepheids we use for kinematical analysis lie at distances $R > 4$ kpc.

In the catalogue of Mróz et al. (2019), some Cepheids are located very far from the Galaxy Centre, at $r > 25$ kpc; it is also better to exclude these from consideration, since at large distances a proper-motion error of about 0.1 mas year^{-1} will lead to tangential velocity errors $e_{V_t} > 10$ km s^{-1} (see Fig. 1b). As a result of the above restrictions, no more than 20 stars are discarded. The total sample contains 800 Cepheids.

3.3 Spectral analysis

According to linear theory (Lin & Shu 1964), the influence of a spiral density wave on the radial V_R and residual tangential velocities ΔV_{circ} has the character of a periodic function and is described by

the following relations:

$$V_R = -f_R \cos \chi,$$

$$\Delta V_{circ} = f_\theta \sin \chi, \qquad (11)$$

where f_R and f_θ are positive-definite amplitudes of the perturbations of the radial and residual tangential velocities, respectively;

$$\chi = m[\cot(i) \ln(R/R_0) - \theta] + \chi_\odot \qquad (12)$$

is the phase of the spiral wave, where m is the number of spiral arms, i is a pitch angle of the spiral pattern, and $\chi_\odot$ is the radial phase of the Sun in a spiral wave. As an analysis of modern high-precision data showed, the periodicities associated with a spiral density wave also appear in vertical velocities W (Bobylev & Bajkova 2015; Rastorguev et al. 2017).

To identify periodicities in the velocities V_R and ΔV_{circ}, we use a modified spectral (periodogram) analysis (Bajkova & Bobylev 2012). Wavelength λ (distance between adjacent pieces of spiral
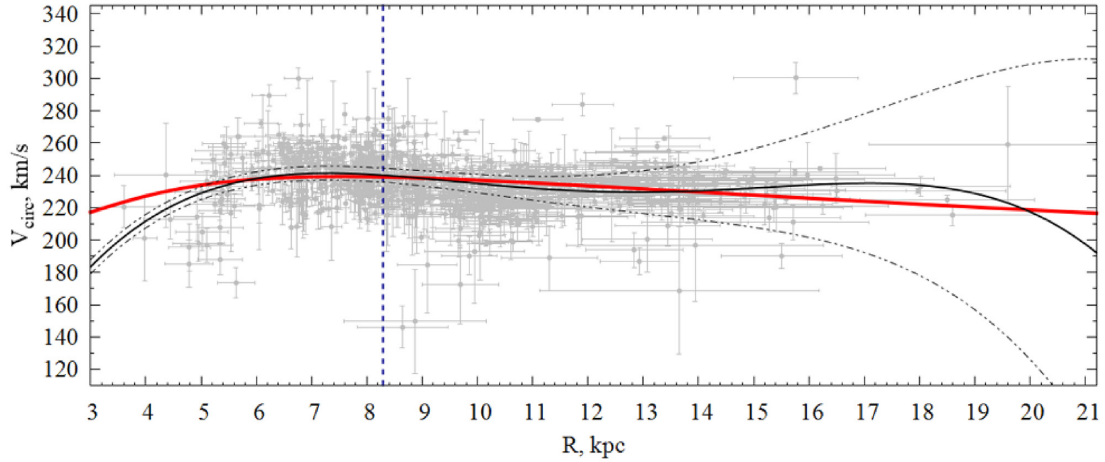
Figure 5. Rotation velocities of Cepheids V_{circ} versus the distance R; the thin solid line shows the Galaxy rotation curve found from these stars (solution 17), while the wide red line shows the rotation curve corresponding to the potential model III (Bajkova & Bobylev 2016). The confidence interval limits corresponding to an error level of 1σ are marked with dashed lines. The vertical line marks the position of the Sun.

arms, counted along the radial direction) is calculated as follows:

$$\frac{2\pi R_0}{\lambda} = m \cot(i). \quad (13)$$

Let there be a series of measured velocities V_{R_n} (these can be V_R or ΔV_{circ} velocities), $n = 1, \ldots, N$, where N is the number of objects. The task of spectral analysis is to extract the periodicity from a data series in accordance with the accepted model describing a spiral density wave with parameters f, λ (or i), and $\chi_\odot$.

As was shown by Bajkova & Bobylev (2012), taking into account the logarithmic nature of the spiral density wave, as well as the positional angles θ_n of objects, our spectral analysis of the series of velocities can be reduced to calculating of the power spectrum of the standard Fourier transform:

$$\bar{V}_{\lambda_k} = \frac{1}{N} \sum_{n=1}^{N} V_n'\left(R_n'\right) \exp\left(-j\frac{2\pi R_n'}{\lambda_k}\right), \quad (14)$$

where $\bar{V}_{\lambda_k}$ is the kth harmonic of the Fourier transform with the wavelength $\lambda_k = D/k$, D is the period of the analysed series,

$$R_n' = R_0 \ln(R_n/R_0),$$

$$V_n'\left(R_n'\right) = V_n\left(R_n'\right) \times \exp(jm\theta_n). \quad (15)$$

The peak value of the power spectrum S_{peak} corresponds to the desired wavelength λ. The pitch angle of the spiral density wave can be found from (13). We find the amplitude and phase of the perturbations as a result of fitting the harmonics with the found wavelength to the measured data. To estimate the amplitude of disturbances, we use the relation

$$f_R(f_\theta) = 2 \times \sqrt{S_{peak}}. \quad (16)$$

3.4 Choice of R_0 value

Currently, a number of works devoted to determining the average value of the Sun's Galactocentric distance have been performed using individual definitions of this quantity, obtained in the last decade by independent methods.

We note several important results, derived as an average over a large number of independent estimates of R_0: for instance, $R_0 =$ 8.0 $\pm$ 0.2 kpc (Vallée 2017a), $R_0 = 8.3 \pm 0.4$ kpc (de Grijs & Bono 2017), or $R_0 = 8.0 \pm 0.15$ kpc (Camarillo et al. 2018).

We also note some of the first-class individual definitions of this quantity made recently. In the work of Abuter et al. (2019), from the analysis of a 16-year-long series of observations of the motion of the S2 star around a supermassive black hole in the centre of the Galaxy, the value $R_0 = 8.178 \pm 0.022$ kpc was found. In the work of Do et al. (2019), based on an independent analysis of the orbit of star S2, the value $R_0 = 7.946 \pm 0.032$ kpc was found. Using data on Galactic masers obtained with the Japanese programme VERA (VLBI Exploration of Radio Astrometry), Hirota et al. (2020) received an estimate of $R_0 = 7.9 \pm 0.3$ kpc. Estimates obtained from the analysis of variable stars are also of interest. From the analysis of VVV (VISTA Variables in the Via Lactea)-based near-infrared RR Lyrae data, Majaess et al. (2018) obtained $R_0 = 8.30 \pm 0.36$ kpc. From the analysis of OGLE-based RR Lyrae data, Griv et al. (2020) obtained $R_0 = 8.28 \pm 0.14$ kpc.

Based on the above results, in the present work we assume the value $R_0 = 8.0 \pm 0.15$ kpc in cases where R_0 is not a definable parameter.

4 RESULTS AND DISCUSSION

4.1 Galaxy rotation

The system of conditional equations (4)–(6) has been solved by the least-squares method with weights of a form inversely proportional to random velocity errors, discarding residuals by the criterion of 3σ.

As can be seen from Fig. 4, with an increase in the delineable unknowns, the confidence region expands significantly with increasing R. The rotation curve is close to flat, which is in good agreement with the conclusion of Mróz et al. (2019). Note that in the catalogue of Mróz et al. (2019) there is a 'flag' parameter indicating whether the star was used in kinematic analysis. The criteria of Mróz et al. (2019) are more stringent compared with (10), since they leave only 773 stars in the sample. Our sample contains about 800 Cepheids with estimates of their age. After applying all the rejection criteria, our final sample contains 788 Cepheids.

Of the four cases presented in the figure, it is better to choose the option in which the rotation curve is closest to flat, in order to provide the most accurate spectral analysis of the residual velocities with a
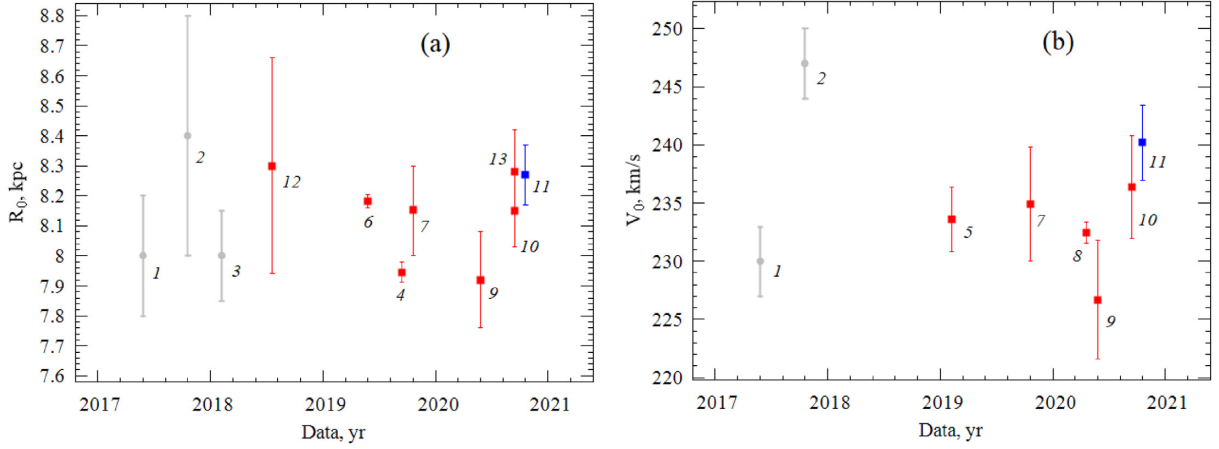
Figure 6. The results of determining (a) distance R_0 and (b) velocity V_0 by various authors, depending on the date of publication; a grey colour indicates the results were obtained as an average, red individual determinations, and blue the result of this work; see also the text.

minimum of false waves. In Fig. 4(a) the curve rises too early (at $R \sim$ 13 kpc). The curve in Fig. 4(d) seems to fit the data better around 12–13 kpc, but indeed with a wider confidence interval and unnecessary wriggles at large Galactocentric distances. As a result, the rotation curves shown in Figs 4(b) and (c) can be used to obtain the residual Cepheid velocities ΔV_{circ} for the purpose of spectral analysis.

For the entire sample of 788 Cepheids, the following kinematic parameters were found:

$$(U_\odot, V_\odot, W_\odot) = (10.1, 13.6, 7.0) \pm (0.5, 0.6, 0.4)\ \mathrm{km\,s^{-1}},$$

$$\Omega_0 = 29.05 \pm 0.15\ \mathrm{km\,s^{-1}\,kpc^{-1}},$$

$$\Omega_0' = -3.789 \pm 0.045\ \mathrm{km\,s^{-1}\,kpc^{-2}},$$

$$\Omega_0'' = 0.722 \pm 0.027\ \mathrm{km\,s^{-1}\,kpc^{-3}},$$

$$\Omega_0''' = -0.087 \pm 0.007\ \mathrm{km\,s^{-1}\,kpc^{-4}},$$

$$R_0 = 8.27 \pm 0.10\ \mathrm{kpc}, \tag{17}$$

where the error of the unit of weight $\sigma_0 = 12.4\ \mathrm{km\,s^{-1}}$ and the Galaxy rotation velocity $V_0 = 240.2 \pm 3.2\ \mathrm{km\,s^{-1}}$. Note that the solution (17) was obtained in such a way that R_0 was also considered an unknown variable. The rotation curve with parameters (17) is shown in Fig. 5.

Based on a sample of 147 masers with trigonometric parallaxes, Reid et al. (2019) found the following values of the two most important kinematic parameters: $R_0 = 8.15 \pm 0.15$ kpc and $\Omega_\odot = 30.32 \pm 0.27\ \mathrm{km\,s^{-1}\,kpc^{-1}}$, where $\Omega_\odot = \Omega_0 + V_\odot/R$. The velocity $V_\odot = 12.24\ \mathrm{km\,s^{-1}}$ was taken from Schönrich, Binney & Dehnen 2010). Reid et al. (2019) used expansion of the linear Galactic rotation velocity into a series.

Based on a similar approach, Hirota et al. (2020) obtained the following estimates from analysis of 99 masers that were observed within the VERA programme: $R_0 = 7.92 \pm 0.16$ (stat.)± 0.3 (syst.) kpc and $\Omega_\odot = 30.17 \pm 0.27$ (stat.)± 0.3 (syst.) $\mathrm{km\,s^{-1}\,kpc^{-1}}$, where $\Omega_\odot = \Omega_0 + V_\odot/R$, and the velocity $V_\odot = 12.24\ \mathrm{km\,s^{-1}}$ was also taken from Schönrich et al. (2010).

Based on 239 Galactic masers with measured trigonometric parallaxes, Bobylev, Krisanova & Bajkova (2020) found the solar velocity components $(U_\odot, V_\odot, W_\odot) = (7.79, 15.04, 8.57) \pm (1.25, 1.25, 1.21)$ $\mathrm{km\,s^{-1}}$ and the following parameters of the Galactic rotation curve: $\Omega_0 = 29.01 \pm 0.33\ \mathrm{km\,s^{-1}\,kpc^{-1}}$, $\Omega_0' = -3.901 \pm 0.069\ \mathrm{km\,s^{-1}}$ $\mathrm{kpc^{-2}}$, $\Omega_0'' = 0.831 \pm 0.032\ \mathrm{km\,s^{-1}\,kpc^{-3}}$, and $V_0 = 236.4 \pm 4.4\ \mathrm{km}$ $\mathrm{s^{-1}}$ for the value of $R_0 = 8.15 \pm 0.12$ kpc found.

Using a sample of 773 classical Cepheids with precise distances coupled with proper motions and line-of-sight velocities from Gaia DR2, Mróz et al. (2019) constructed the rotation curve of the Milky Way up to a distance of $R \sim 20$ kpc. These authors found the rotation velocity of the Sun to be $V_0 = 233.6 \pm 2.8\ \mathrm{km\,s^{-1}}$ for an adopted $R_0 = 8.122 \pm 0.031$ kpc. It should be noted that the rotation velocity V_0 found by us (17) is in very good agreement with the result of Mróz et al. (2019), obtained from the analysis of almost the same stars.

In a recent work by Ablimit et al. (2020), around 3500 classical Cepheids from various sources, including Mróz et al. (2019) and Skowron et al. (2019), were used to construct the rotation curve of the Galaxy over the distance interval $R = 4$–19 kpc. The circular rotation velocity of the solar neighborhood was obtained equal to $V_0 = 232.5 \pm 0.9\ \mathrm{km\,s^{-1}}$ (for an adopted $R_0 = 8.122 \pm 0.031$ kpc), which is in good agreement with our estimate.

Further, we assume that the true r_{t} and the adopted distance r are related as $r_{\mathrm{t}} = r/p$, where p is the distance-scale correction factor. The value of the coefficient p is determined by the internal agreement of the data, namely by the agreement of the line-of-sight and tangential velocities. There are two ways to search for the value of the coefficient p: either by solving the basic kinematic equations (4)–(6), where it will act as an unknown (Rastorguev et al. 2017), or by comparing the values of the first derivative Ω_0' obtained only from the analysis of line-of-sight velocities, $\Omega_0'(r)$, and only tangential velocities, $\Omega_0'(\mu)$, rather than $p = \Omega_0'(\mu)/\Omega_0'(r)$ (Zabolotskikh, Rastorguev & Dambis 2002).

We defined the value of the factor p both for the entire sample and for subsamples of different ages. As a result, we found that the coefficient p always has approximately the same value, equal to ~ 0.9. On this basis, it is concluded that the distances r of the analysed Cepheids, calculated on the basis of the period–luminosity relation, must be extended by about 10 per cent.

The results of determining R_0 and V_0 by various authors are given in Fig. 6, where the results are marked with the following numbers: (1) Vallée (2017a), (2) de Grijs & Bono (2017), (3) Camarillo et al. (2018), (4) Do et al. (2019), (5) Mróz et al. (2019), (6) Abuter et al. (2019), (7) Reid et al. (2019), (8) Ablimit et al. (2020), (9) Hirota et al. (2020), (10) Bobylev et al. (2020), (11) this work, (12) Majaess et al. (2018), (13) Griv et al. (2020).

Fig. 5 gives two rotation curves. One corresponds to solution (17). The second curve corresponds to the axisymmetric gravitational potential model III (a modified NFW model) from the work of

Table 1. The parameters of the spiral density wave found from samples of Cepheids from three age intervals for the present moment of time.

Parameters	$t < 90$ Myr	$t: 90-120$ Myr	$t > 120$ Myr
λ_R, kpc	2.5 ± 0.3	3.0 ± 0.6	5.1 ± 1.1
f_R, km s^{-1}	12.0 ± 2.3	9.2 ± 2.5	6.5 ± 1.5
i_R, deg	-10.8 ± 3.1	-13.1 ± 3.5	-21 ± 4
$(\chi_\odot)_R$, deg	26 ± 11	52 ± 10	-8 ± 4
λ_θ, kpc	2.7 ± 0.5	2.6 ± 0.7	4.8 ± 1.4
f_θ, km s^{-1}	8.9 ± 2.5	9.6 ± 2.7	7.5 ± 1.5
i_θ, deg	-11.8 ± 3.1	-11.6 ± 3.8	-20 ± 5
$(\chi_\odot)_\theta$, deg	58 ± 12	-51 ± 12	12 ± 6

Bajkova & Bobylev (2016):

$$V_{\text{circ}}^2 = \frac{M_b R^2}{\left(R^2 + b_b^2\right)^{3/2}} + \frac{M_d R^2}{[R^2 + (a_d + b_d)^2]^{3/2}}$$
$$+ M_h \left[\frac{\ln(1 + R/a_h)}{R} - \frac{1}{R + a_h}\right] + const, \quad (18)$$

where M_b, M_d, and M_h are the masses of the bulge, disc, and halo respectively, while b_b, a_d, b_d, and a_h are the scalelengths (in kpc) of the corresponding Galactic components. The gravitational potential is expressed in units of 100 km^2 s^{-2}, the lengths in kpc, and the masses in Galactic mass units $M_g = 2.325 \times 10^7$ M$_\odot$ providing the value of the gravitational constant $G = 1$. The term *const* is needed here to match the solar rotation velocity V_0 accurately in this work and in the work of Bajkova & Bobylev (2016) (*const* = -4.8 km^2 s^{-2}).

To construct a curve, it is necessary to substitute the following values of seven parameters into this formula (18): $M_b = 44\,300$ (M_g), $b_b = 0.2672$ kpc, $M_d = 279\,800$ (M_g), $a_d = 4.40$ kpc, $b_d = 0.3084$ kpc, $M_h = 1\,247\,400$ (M_g), $a_h = 7.7$ kpc.

For spectral analysis of residual circular velocities ΔV_{circ}, it is important that they are obtained with a relatively smooth rotation curve. As can be seen from Fig. 5, the curve (18) can be used to obtain residual circular velocities for a very wide range of distances $R > 4$ kpc. The applicability of the rotation curve corresponding to the solution (17) is limited by the interval R: 4–20 kpc. In spectral analysis, we use both of the rotation curves described above for mutual control.

4.2 Spiral density-wave parameters

Spectral analysis was performed for Cepheids from three samples of different ages. The age boundaries were chosen so as to ensure an approximately equal number of stars in the samples. For each sample, the spiral density-wave parameters were obtained for two cases. In

the first case, spectral analysis was performed for the present moment in time. In the second case, the position and speeds of each Cepheid were taken at the time of their birth. That is, a Galactic orbit in the past was constructed for each star, in accordance with an estimate of its age. To construct Galactic orbits in the past, an axisymmetric model of the gravitational potential of the Galaxy was used (a modified NFW model from Bajkova & Bobylev 2016).

The first sample contains 254 stars satisfying the condition $t \leq 90$ Myr. The average age of these relatively young Cepheids is $\bar{t} = 66$ Myr.

The second sample contains 249 stars with ages in the interval 90–120 Myr. The average age of these Cepheids is $\bar{t} = 105$ Myr.

The third sample contains 304 stars selected under the condition $t > 120$ Myr. The average age of these Cepheids is $\bar{t} = 165$ Myr.

Fig. 7 shows the X, Y distribution of three samples of Cepheids at the present time and in the past according to the age of each star. Parameters given in Fig. 7 for a four-arm spiral pattern were found by Bobylev & Bajkova (2014) from masers with measured trigonometric parallaxes. In the figure, the following segments of spiral arms are numbered in Roman numerals: I the Scutum arm, II the Carina–Sagittarius arm, III the Perseus arm, IV the outer arm.

The results of the spectral analysis of Cepheids are reflected in Tables 1–2, as well as in Figs 8–11.

Table 1 gives the parameters of the spiral density wave found from samples of Cepheids from three age intervals for the current moment of time. In Table 2, similar values are given for four samples of Cepheids calculated using their past positions. In Table 2, a column with the results obtained for the entire sample is added.

One of the most important parameters determined on the basis of spectral analysis is the wavelength λ. With the found value λ, the pitch angle i is calculated using the relation (13). As can be seen from the first and second columns of Tables 1–2, for samples of Cepheids younger than 120 Myr, the values of λ lie in the range 2.4–3.0 kpc (this means that i is in the range $[-13°-10°]$ for a four-arm pattern model, $m = 4$).

The values of λ_R and λ_θ found from a sample of Cepheids older than 120 Myr for the current moment of time (Table 1) are very different from similar values found from younger Cepheids. This problem is eliminated only in the case of an analysis of the velocities of the old Cepheids calculated at the time of their birth (Table 2 and Figs 10–11).

Fig. 8 shows the radial V_R and residual tangential ΔV_{circ} velocities at the present time obtained for a sample of young ($t \leq 90$ Myr) Cepheids and their spower spectra. For the same Cepheids, Fig. 9 gives the radial V_R and residual tangential ΔV_{circ} velocities versus the distance R at the present time and in the past, where the periodic curves show the effect of a spiral density wave. The first column of Table 1 gives the values of the spiral-wave parameters found using

Table 2. Parameters of a spiral density wave found from samples of Cepheids from four age intervals in the past.

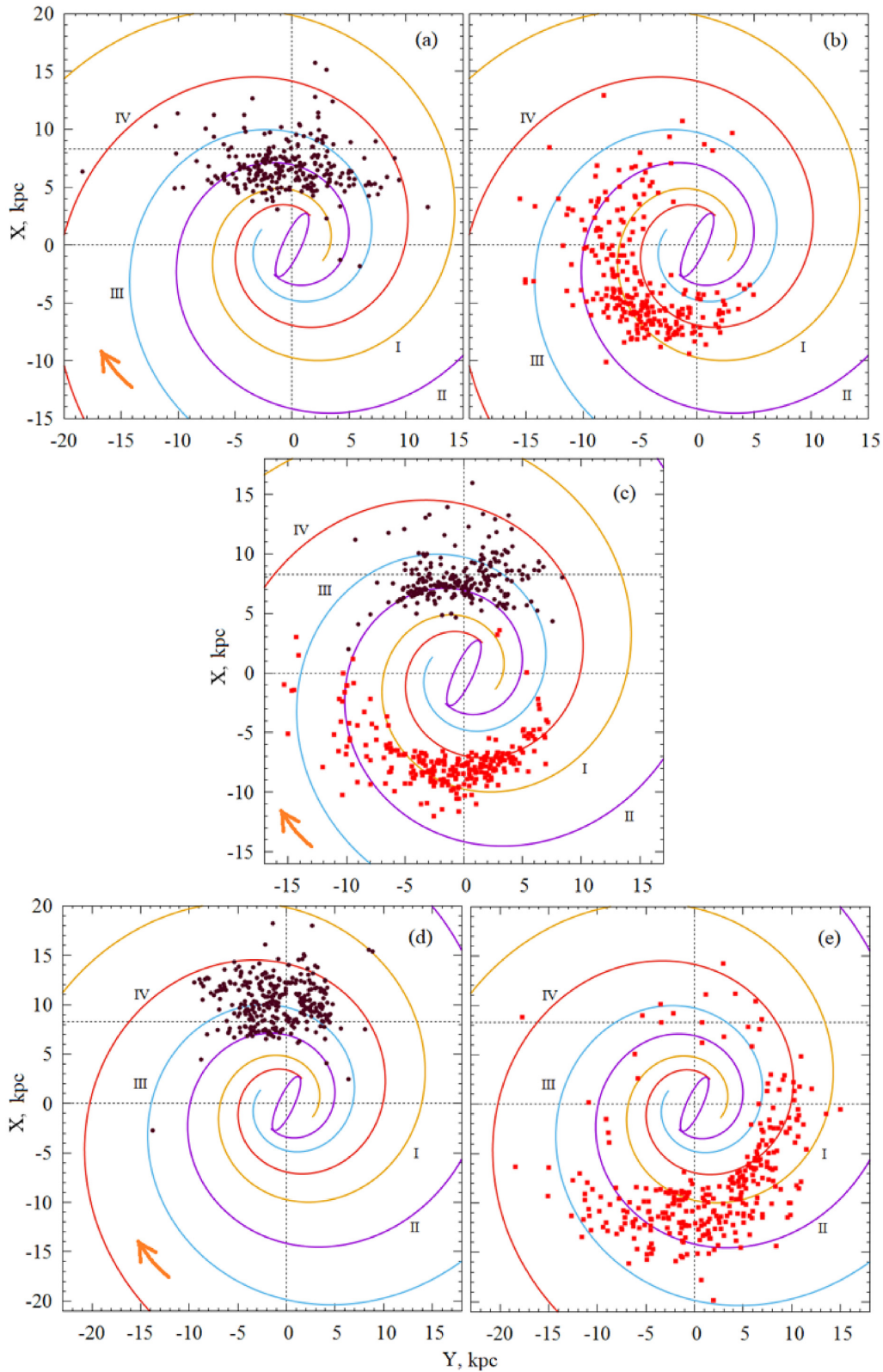| Parameters	$t < 90$ Myr	$t: 90-120$ Myr	$t > 120$ Myr	Whole sample
λ_R, kpc	2.6 ± 0.5	2.4 ± 0.8	2.7 ± 0.8	2.3 ± 0.4
f_R, km s^{-1}	12.9 ± 2.6	13.2 ± 3.0	7.9 ± 3.5	9.0 ± 2.1
i_R, deg	-11.6 ± 3.4	-10.5 ± 3.6	-11.8 ± 3.3	-10.0 ± 2.4
$(\chi_\odot)_R$, deg	-74 ± 15	-44 ± 17	-73 ± 18	-50 ± 10
λ_θ, kpc	2.9 ± 0.6	2.4 ± 0.7	2.7 ± 0.8	2.7 ± 0.5
f_θ, km s^{-1}	8.3 ± 2.6	11.7 ± 3.1	5.0 ± 3.2	5.9 ± 2.4
i_θ, deg	-12.7 ± 3.5	-10.5 ± 3.6	-11.8 ± 3.3	-11.9 ± 2.5
$(\chi_\odot)_\theta$, deg	60 ± 16	60 ± 18	-33 ± 14	-81 ± 12

Figure 7. The distribution on the Galactic plane *X*, *Y* of the youngest Cepheids (a) at the present time and (b) in the past according to the age of each star, (c) middle-aged Cepheids, samples of old Cepheids (d) at the present time and (e) in the past. A four-arm spiral pattern with a pitch angle of −13° (Bobylev & Bajkova 2014) is given, the spiral arms are numbered in Roman numerals, the orange arrow shows the direction of the Galaxy's rotation, the purple dots represent the current positions of the Cepheids, and the red dots represent their positions in the past.
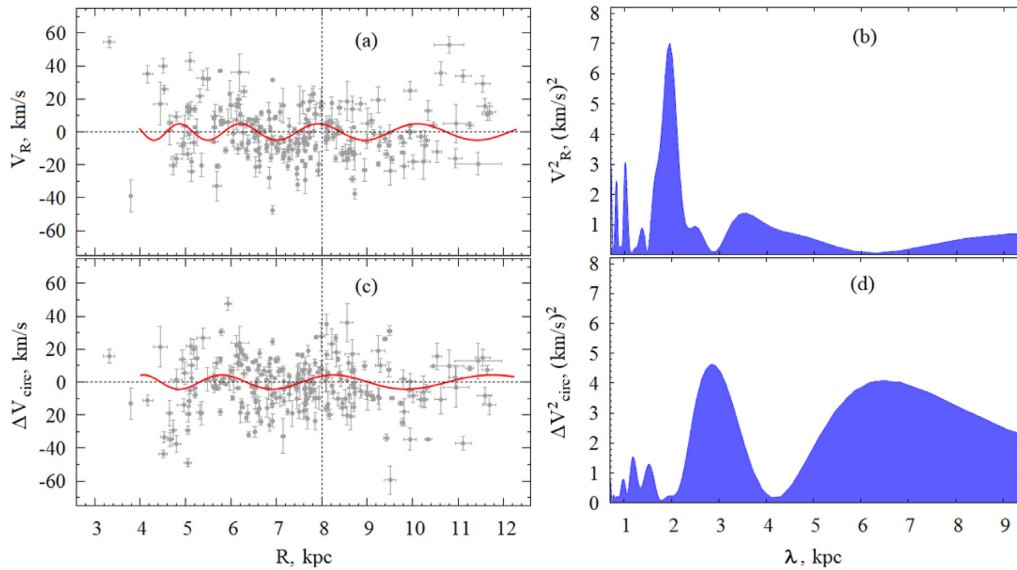
Figure 8. In the left-hand panels, (a) radial V_R and (c) residual tangential ΔV_{circ} velocities of young ($t \leq 90$ Myr) Cepheids are shown. The velocities are given with error bars; the continuous periodic curves corresponding to the peaks of the power spectra (the spiral density wave) are given in red. The vertical dotted line marks the position of the Sun. In the right-hand panels, the corresponding power spectra (b) and (d) are shown.
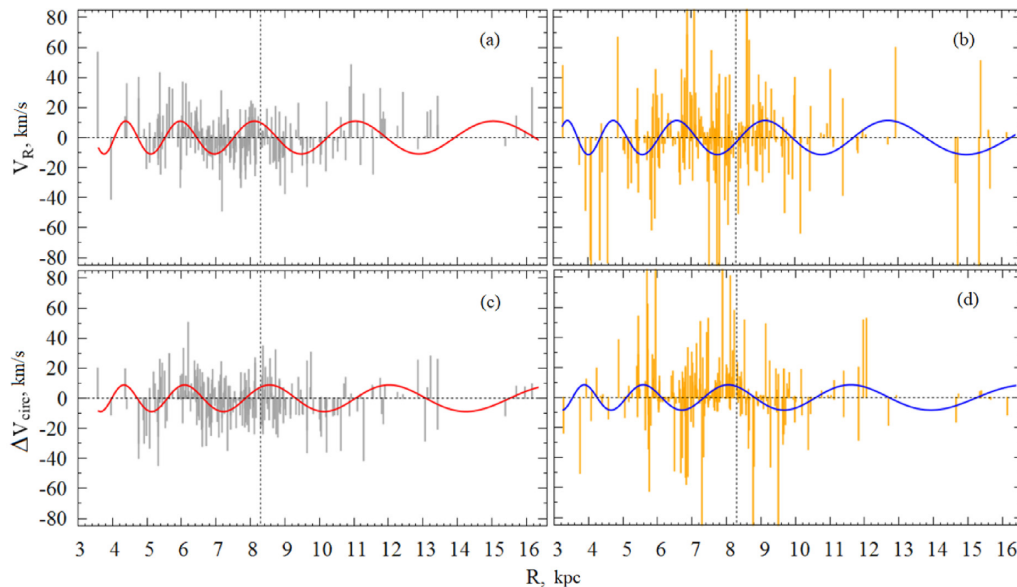

Figure 9. The radial V_R velocities of young ($t \leq 90$ Myr) Cepheids in (a) the present and (b) the past, and their residual tangential ΔV_{circ} velocities in (c) the present and (d) the past. The continuous periodic curves corresponding to the peaks of the power spectra (the spiral density wave) are shown in red (in the present) and blue (in the past). The vertical dotted line marks the position of the Sun.

the young ($t \leq 90$ Myr) Cepheids. It should be noted that, both for the sample of young Cepheids and for Cepheids of intermediate age, the values of the parameters of the spiral wave indicated in both tables are close. Therefore, illustrations for Cepheids of intermediate age are not given.

In Fig. 10, for the sample of old ($t > 120$ Myr) Cepheids, radial V_R and residual tangential ΔV_{circ} velocities are given at the present time, along with their power spectra. The radial V_R and residual tangential ΔV_{circ} velocities are shown in Fig. 11 at the present time and in the past.

Another important parameter to be determined on the basis of spectral analysis is the amplitude of the perturbations f_R or f_θ. If

we take the peak values of the squares of velocities from the power spectra in Fig. 8 or Fig. 10, then the values f_R or f_θ (indicated in the tables) can be found by formula (16).

An analysis of modern data shows that, in a wide region of the solar neighbourhood, the velocities f_R and f_θ are usually 4–9 km s^{-1} and the wavelength λ is in the range 2–3 kpc.

Thus, from 130 maser sources with measured trigonometric parallaxes in the work of Rastorguev et al. (2017), the following values were found: $f_R = 6.9 \pm 1.4$ km s^{-1} and $f_\theta = 2.8 \pm 1.0$ km s^{-1}, solar phase $\chi_\odot = -125° \pm 10°$. From 239 Galactic masers with measured trigonometric parallaxes in the work of Bobylev et al. (2020), $f_R = 7.0 \pm 0.9$ km s^{-1} and $f_\theta = 3.8 \pm 1.1$ km s^{-1} were found.

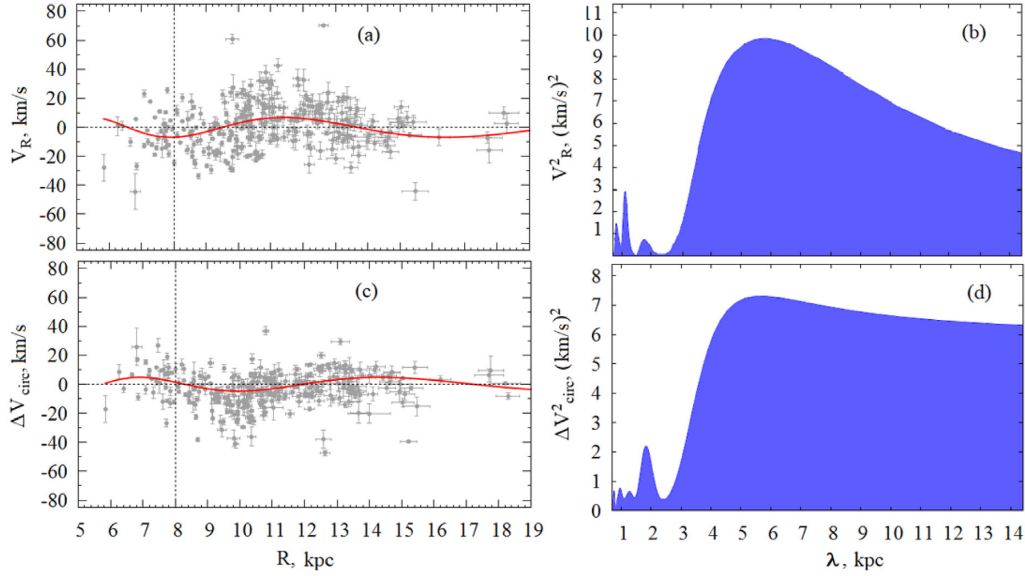**Figure 10.** In the left-hand panels, (a) radial V_R and (c) residual tangential ΔV_{circ} velocities of old ($t > 120$ Myr) Cepheids are shown. The velocities are given with error bars; the continuous periodic curves corresponding to the peaks of the power spectra (the spiral density wave) are given in red. The vertical dotted line marks the position of the Sun. In the right-hand panels, the corresponding power spectra (b) and (d) are shown.
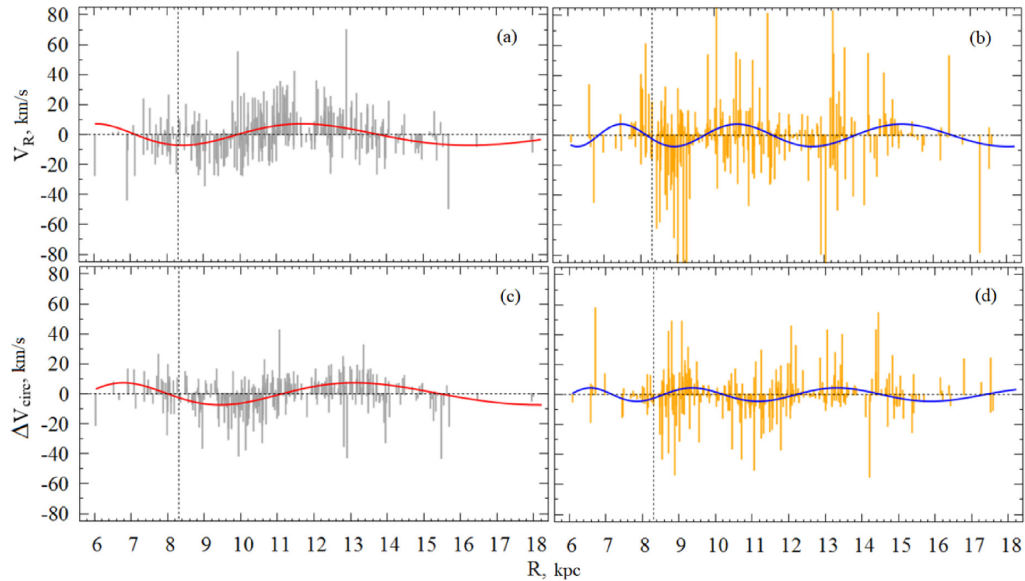
Figure 11. The radial V_R speeds of the old ($t > 120$ Myr) Cepheids in (a) the present and (b) the past, with their residual tangential ΔV_{circ} speeds in (c) the present and (d) the past. The continuous periodic curves corresponding to the peaks of the power spectra (the spiral density wave) are shown in red (in the present) and blue (in the past). The vertical dotted line marks the position of the Sun.

From about 500 OB stars of the Gaia DR2 Catalogue, Bobylev & Bajkova (2018) determined $f_R = 7.1 \pm 0.3$ km s^{-1} and $f_\theta = 6.5 \pm 0.4$ km s^{-1}, and $\lambda_R = 2.3 \pm 0.2$ kpc and $\lambda_\theta = 2.3 \pm 0.2$ kpc, $(\chi_\odot)_R = -135° \pm 5°$ and $(\chi_\odot)_\theta = -123° \pm 8°$. From a sample of open clusters younger than 50 Myr, Bobylev, Bajkova & Shirokova (2016) determined $f_R = 7.7 \pm 1.4$ km s^{-1} and $f_\theta = 5.6 \pm 1.6$ km s^{-1}, $\lambda_R = 2.1 \pm 0.5$ kpc and $\lambda_\theta = 2.6 \pm 0.5$ kpc, $(\chi_\odot)_R = -85° \pm 10°$ and $(\chi_\odot)_\theta = -62° \pm 9°$.

From about 200 Cepheids from the *Hipparcos* Catalogue, Bobylev & Bajkova (2012) found $f_R = 6.8 \pm 0.7$ km s^{-1} and $f_\theta = 3.3 \pm 0.5$ km s^{-1}, $\lambda = 2.0 \pm 0.1$ kpc, $\chi_\odot = -193° \pm 5°$. We also note the new values of $f_R = 4.6 \pm 0.7$ km s^{-1} and $f_\theta = 1.1 \pm 0.4$ km s^{-1}, obtained

in a recent work by Loktin & Popova (2019) from the analysis of modern data on open star clusters.

Note that (Burton 1971) calculated the expected values for the perturbation velocities $f_R \approx 8$ km s^{-1} and $f_t \approx 6$ km s^{-1} for $R = 8$ kpc.

The results of determining f_R, f_θ and $\lambda_R, \lambda_\theta$ by various authors are given in Fig. 12, where the results are marked with the following numbers: (1) Rastorguev et al. (2017), (2) Bobylev & Bajkova (2018), (3) Bobylev & Bajkova (2012), (4) Loktin & Popova (2019), (5) Bobylev et al. (2020), (6) Bobylev et al. (2016), (7) and black square: Burton (1971); results of this work from the last column of Table 2 are shown in blue, while those from the first and second columns of Table 1 are shown in grey.
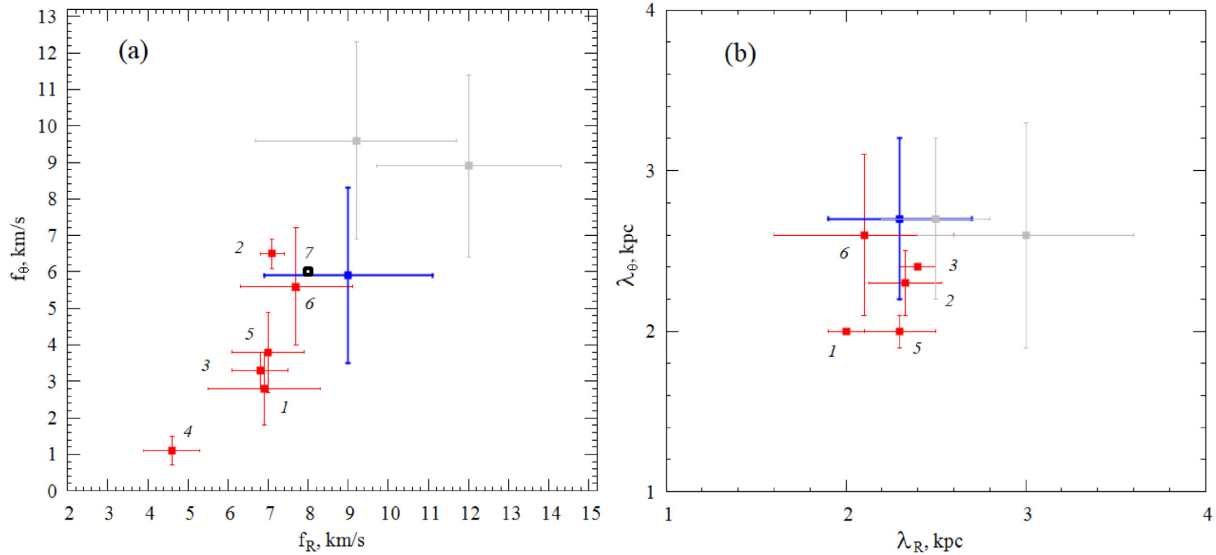
Figure 12. The results of determining the velocities (a) f_R and f_θ and (b) λ_R and λ_θ by various authors are shown in red and black, while blue and grey denote the results of this work; see also the text.

Currently, there is no single generally accepted model of the spiral structure of the Galaxy. Theorists usually use the simplest two-arm model with a pitch angle of 5–7°. Modern data on the distribution of clouds of neutral hydrogen, ionized hydrogen, and maser sources speaks instead of a four-arm model with a pitch angle of 10–14°. Reviews on this issue can be found, for example, in the works Hou & Han (2014) or Vallée (2017c). In this work, we adhere to the four-arm spiral pattern model with the parameters we found in previous works from the spatial and kinematical analysis of maser sources (Bobylev & Bajkova 2014).

In work of Dambis et al. (2015), an analysis of the spatial distribution of a large sample of classical Cepheids yielded estimates of the pitch angle of the four-arm spiral pattern $i = -9.5° \pm 0.1°$ and the solar phase $\chi_\odot = -121° \pm 3°$.

The model of the global four-arm spiral pattern in the Galaxy is defended, for example, in the works of Vallée (2017b, 2018). Some authors have preferred (before the appearance of more high-precision data) to consider individual segments of spiral arms with individual pitch angles (Nikiforov & Veselova 2018). In these models, the pitch angle lies in the range from $-10°$ to $-15°$.

Light absorption strongly distorts the spatial distribution of objects and makes it difficult not only to determine their photometric distances but also to calibrate the PLR even by high-precision trigonometric distances. To determine the absolute magnitude, it is necessary to know the colour excesses, and for the Cepheids of the Milky Way this is a much more serious problem than for stars of constant brightness (Rastorguev et al. 2013; Lazovik & Rastorguev 2020) or for Large Magellanic Cloud (LMC) Cepheids. Supposing a unified absorption law, we can solve these problems and reduce the effect of differential absorption by using two-colour Wesenheit indices (W_{VI} as an example) instead of absolute magnitudes (Madore 1976). To use Wesenheit indexes of Cepheids instead of PLR, we should know the 'period–normal colour' relation, which reflects the shape and width of the instability strip and depends strongly on the metallicity of young populations. In addition, the use of Wesenheit indices or tricolour indices like Q_{UBV} to reduce the effects of differential absorption is justified only for a small optical depth of dust in the broad-band (heterochromic)

photometry, which does not take place for the Milky Way disc in the optical.

The problem of calibrating PLRs and estimating photometric distances is additionally complicated by a noticeable difference in the absorption laws in the Milky Way galaxy (Fitzpatrick & Massa 2007, 2009), differing, first of all, by the value $R_V = A_V/E_{B-V}$, which varies from 2–6. That is why the photometric distances of the objects in the Galactic disc, determined by optical data, can suffer strongly from both random and hard-to-account for systematic errors.

It is for these reasons that, in recent years, photometric data in the NIR/MIR (Two-Micron All-Sky Survey (2MASS), AllWISE (Wide-field Infrared Surway Explorer All-Sky Data Release), *Spitzer* and other projects) have been used to determine the photometric distances of objects, including Cepheids. For example, light absorption (expressed in magnitudes) in the K_s (2MASS) band is $A_{K_s} \approx 0.078(\pm0.004) \cdot Av$, and in the WISE $W1$, $W2$ bands is $A_{W1} \approx 0.039(\pm 0.004) \cdot Av$ and $A_{W2} \approx 0.026(\pm 0.004) \cdot Av$, respectively (Wang & Chen 2019). As is well known, average specific absorption a_V in the Galaxy plane is about 1.5 mag kpc^{-1} and, as a result, up to distances of 5 kpc in the $W2$ band, absorption does not exceed 0.20 mag (which is comparable with the internal scatter of the PLR) and the effect of differences in the absorption laws is negligible. It should also be noted that the study of structures in the Galaxy, such as a spiral patterns, based on the spatial distribution of objects is greatly affected by selection effects due to interstellar extinction, even in the IR. However, these selection effects do not affect the kinematics at all, which justifies the kinematic analysis of the spiral structure performed in this work.

As for microlensing effects, it should be borne in mind that for bulge stars these effects should be taken into account, due to the huge number of observed stars (this is exactly what the results of the OGLE project discovered). The total sample size of Cepheids is negligible compared with the sample of bulge stars studied in OGLE and, even with the same lensing probability, the average expected number of lensings for the entire sample is much less than unity. Also, the lensing event itself, lasting some tens of days, in principle could not distort either the estimate of the period (since the photometric monitoring of Cepheids lasts much longer than this time) or the

results of precision astrometric measurements by *Gaia*, conducted for about 30 months.

Most recently, the latest version of the Gaia Early Data Release 3 (Brown et al. 2020; Lindegren et al. 2020) catalogue was published. It clarifies the values of trigonometric parallaxes and proper motions for about 1.5 billion stars by about 30 per cent. The radial velocities are simply copied from the Gaia DR2 Catalogue. We hope that the use of new data will not have a fundamental impact on the conclusions of this work.

Flat rotation curves of young objects reaching distances of about 15–20 kpc from the Galactic Centre, derived in numerous works cited here, show an almost linear increase in effective mass with distance. A simple estimate of the effective mass within a radius of 20 kpc for a rotation velocity of 220–230 km s^{-1} leads to $(2.3 \pm 0.3) \times 10^{11}$ solar masses. Even to this mass, the dark matter gives the significant contribution, which only dominates with a further increase in distance. Its total contribution to the mass of the Galaxy and the local density of gravitating matter can be estimated only by modelling the gravitational potential, which takes into account the contribution of all structural components of the Galaxy to the rotation curve. In particular, this was done in the cited works of Ablimit et al. 2020) and Bajkova & Bobylev (2016). In the latter work, the parameters of the density laws were derived from the kinematical study not only of disc objects but also of very distant halo objects, and therefore they are considered more reliable compared with those based only on objects within 15–20 kpc from the Galactic Centre.

In this article, it was shown that the rotation curve of Cepheids is approximated well by the theoretical three-component model III from Bajkova & Bobylev (2016). Taking the parameter estimates of the NFW model and the appropriate errors, we can easily derive an estimate of the contribution of DM to the total local density of gravitating matter: $\rho_{\rm DM} \approx 0.0114^{+0.0078}_{-0.0049}$ M$_\odot$ pc^{-3}, which is 5–20 per cent of the contribution of baryonic matter (0.101 M$_\odot$ pc^{-3}), according to the latest estimate made by the authors of the Besancon model of the Milky Way (Mor et al. 2018), based on the entire set of observational data. Our estimate of DM's contribution, in particular, is in excellent agreement with those of Mor et al. (2018) (0.012 ± 0.001 M$_\odot$ pc^{-3}), de Salas et al. (2019) (0.008 − 0.011 M$_\odot$ pc^{-3}), and Ablimit et al. (2020) (0.0105 ± 0.0012 M$_\odot$ pc^{-3}). Note also that all the above estimates agree with an upper limit on the DM contribution to the local density in the Milky Way galaxy (0.027 M$_\odot$ pc^{-3}), made on the basis of a completely different approach – the analysis of Galacto-vertical oscillations of Cepheids (Dambis 2004) and young open clusters (Dambis 2003).

5 CONCLUSIONS

The spatial and kinematic properties of a large sample of classical Cepheids with proper motions and line-of-sight velocities from the Gaia DR2 Catalogue were studied. For this, we used data from the works of Mróz et al. (2019) and Skowron et al. (2019). The final sample contains about 800 Cepheids. For each of them there are estimates of distance and also age.

The parameters of Galactic rotation were found over the entire sample of Cepheids: the linear speed of rotation of the Galaxy at a solar distance amounted to $V_0 = 240 \pm 3$ km s^{-1}. Moreover, the distance from the Sun to the axis of rotation of the Galaxy was found to be equal to $R_0 = 8.27 \pm 0.10$ kpc. We found that the distance-scale correction factor p for both the entire sample and subsamples of different ages has approximately the same value, equal to ∼0.9. On this basis, it is concluded that the distances r of the analysed

Cepheids, calculated on the basis of the period–luminosity relation, must be extended by about 10 per cent.

We performed a spectral analysis of both radial, V_R, and residual tangential velocities, $\Delta V_{\rm circ}$, of Cepheid samples of different ages. For each sample, the parameters of the spiral density wave were obtained for two cases. In the first case, spectral analysis was performed for the present moment of time. In the second case, the position and speed of the Cepheids were taken at the time of their birth. That is, a Galactic orbit in the past was constructed for each star, in accordance with an estimate of its age.

A spectral analysis of radial and tangential velocities showed that, for samples of Cepheids younger than 120 Myr, both at the present time and in the past, we obtain close estimates of the parameters of the spiral density wave. The value of the wavelength $\lambda_{R,\theta}$ lies in the range [2.4–3.0] kpc, the pitch angle $i_{R,\theta}$ lies in the range $[-13°, -10°]$ for the four-arm pattern model, the amplitude of the radial perturbations is $f_R \sim 12$ km s^{-1}, and that of the tangential perturbations is $f_\theta \sim 9$ km s^{-1}. These values are in agreement with the results of the analysis of other young objects of the Galaxy (for example, maser sources or OB stars).

However, the sampling rates of older Cepheids (over 120 Myr) at the present time give the wavelength $\lambda_{R,\theta} \sim 5$ kpc (hence $i \sim 20°$). This value contradicts the known results. This means that a lot of time has passed since the birth of these Cepheids in the spiral arms, they are significantly removed from their place of birth, and at present the sample does not have coherent properties. An analysis of positions and velocities of old Cepheids (more than 120 Myr), calculated by integrating their orbits backward in time, made it possible to determine significantly more reliable parameters of the spiral density wave: wavelength $\lambda_{R,\theta} = 2.7$ kpc, and amplitudes of radial and tangential perturbations $f_R = 7.9$ km s^{-1} and $f_\theta = 5$ km s^{-1}, respectively.

DATA AVAILABILITY

The data underlying this article will be shared on reasonable request to the corresponding author.

REFERENCES

Abbott T. M. C. et al., 2019, ApJ, 872, L30
Ablimit I., Zhao G., Flynn C., Bird S. A., 2020, ApJ, 895, L12
Abuter R. et al. (Gravity Collaboration), 2019, A&A, 625, L10
Alard C., 2001, A&A, 379, L44
Anderson R. I., Saio H., Ekstrom S., Georgy C., Meynet G., 2016, A&A, 591, A8
Babusiaux C., Gilmore G., 2005, MNRAS, 358, 1309
Bajkova A. T., Bobylev V. V., 2012, Astron. Lett., 38, 549
Bajkova A. T., Bobylev V. V., 2016, Astron. Lett., 42, 567
Benjamin R. A. et al., 2003, PASP, 115, 953
Berdnikov L. N., Dambis A. K., Vozyakova O. V., 2000, A&AS, 143, 211
Betoule M. et al., 2014, A&A, 568, 22
Bhattacharjee P., Chaudhury S., Kundu S., 2014, ApJ, 785, 63
Bobylev V. V., 2013a, Astron. Lett., 39, 753
Bobylev V. V., 2013b, Astron. Lett., 39, 819

Bobylev V. V., Bajkova A. T., 2012, Astron. Lett., 38, 638
Bobylev V. V., Bajkova A. T., 2014, MNRAS, 437, 1549
Bobylev V. V., Bajkova A. T., 2015, MNRAS, 447, L50
Bobylev V. V., Bajkova A. T., 2018, Astron. Lett., 44, 675
Bobylev V. V., Bajkova A. T., Shirokova K. S., 2016, Astron. Lett., 42, 721
Bobylev V. V., Krisanova O. I., Bajkova A. T., 2020, Astron. Lett., 46, 439
Bono G., Marconi M., Cassisi S., Caputo F., Gieren W., Pietrzynsky G., 2005, ApJ, 621, 966
Brown A. G. A. et al. (Gaia Collaboration), 2018, A&A, 616, A1
Brown A. G. A. et al. (Gaia Collaboration), 2020, preprint (arXiv:2012.01533)
Burton W. B., 1971, A&A, 10, 76
Camarillo T., Varun M., Tyler M., Bharat R., 2018, PASP, 130, 4101
Caputo F., Marconi M., Musella I., 2000, A&A, 354, 610
Chemin L., Renaud F., Soubiran C., 2019, A&A, 578, 14
Churchwell E. et al., 2009, PASP, 121, 213
Clemens D. P., 1985, ApJ, 295, 422
Dambis A. K., 2003, preprint (astro-ph:0303461)
Dambis A. K., 2004, in Kurtz D. W., Pollard K. R., eds, Variable Stars in the Local Group, IAU Colloquium 193, Proc. Conf. 6–11 July 2003, Christchurch, New Zealand, ASP Conf. Proc. 310. Astronomical Society of the Pacific, San Francisco, p. 158
Dambis A. K. et al., 2015, Astron. Lett., 41, 489
de Grijs R., Bono G., 2017, ApJS, 232, 22
de Salas P. F., Malhan K., Freese K., Hattori K., Valluri M., 2019, J. Cosmol. Astroparticle Phys., 10, 37
Do T. et al., 2019, Science, 365, 664
Efremov Yu. N., 2003, Astron. Rep., 47, 1000
Feast M., Whitelock P., 1997, MNRAS, 291, 683
Fitzpatrick E. L., Massa D., 2007, ApJ, 663, 320
Fitzpatrick E. L., Massa D., 2009, ApJ, 699, 1209
Frink S., Fuchs B., Wielen R., 1995, Astron. Gesellschaft Abstract Ser., 11, 196
Gnaciński P., 2019, Astron. Nachr., 340, 787
Griv E., Gedalin M., Pietrukowicz P., Majaess D., Jiang I.-G., 2020, MNRAS, 499, 1091
Groenewegen M. A. T., 2018, A&A, 619, A8
Hammersley P. L., Garzon F., Mahoney T., Calbet X., 1994, MNRAS, 269, 753
Hipparcos Tycho Catalogues, 1997, ESA SP–1200
Hirota T. et al., 2020, PASJ, 72, 50
Hou L. G., Han J. L., 2014, A&A, 569, 125
Joy A. H., 1939, ApJ, 89, 356
Kawata D., Baba J., Ciuca I., Cropper M., Grand R. J. J., Hunt J. A. S., Seabroke G., 2018, MNRAS, 479, L108
Lazovik Ya. A., Rastorguev A. S., 2020, AJ, 160, 136
Leavitt H. S., 1908, Annals of Harvard College Observatory, 60, 87
Leavitt H. S., Pickering E. C., 1912, Harvard College Observatory Circular, 173, 1
Lin C. C., Shu F. H., 1964, ApJ, 140, 646
Lindegren L. et al. (Gaia Collaboration), 2018, A&A, 616, 2
Lindegren L. et al. (Gaia Collaboration), 2020, preprint (arXiv:2012.03380)
Loktin A. V., Popova M. E., 2019, Astrophys. Bulletin, 74, 270
López-Corredoira M., Cabrera-Lavers A., Gerhard O. E., 2005, A&A, 439, 107
Madore B. F., 1976, Royal Greenwich Observatory Bulletin, 182, 153
Madore B. F., 1982, ApJ, 253, 575
Mainzer A. et al., 2011, ApJ, 731, 53
Majaess D., Dekany I., Hajdu G., Minniti D., Turner D., Gieren W., 2018, Ap&SS, 363, 127

Majaess D. J., Turner D. G., Lane D. J., 2009, MNRAS, 398, 263
Mel'nik A. M., Dambis A. K., Rastorguev A. S., 1999, Astron. Lett., 25, 518
Mel'nik A. M., Rautiainen P., Berdnikov L., Dambis A. K., Rastorguev A. S., 2015, Astron. Nachr., 336, 70
Metzger M. R., Caldwell J. A. R., Schechter P. L., 1998, AJ, 115, 635
Mor R., Robin A. C., Figueras F., Antoja T., 2018, A&A, 620, 79
Mróz P. et al., 2019, ApJ, 870, L10
Muraveva T., Delgado H. E., Clementini G., Sarro L. M., Garafalo A., 2018, MNRAS, 481, 1195
Nikiforov I.I, Veselova A. V., 2018, Astron. Lett., 44, 81
Nishiyama S. et al., 2005, ApJ, 621, L105
Perlmutter S. et al., 1997, ApJ, 483, 565
Perlmutter S. et al., 1999, ApJ, 517, 565
Pojmański G., 2002, Acta Astron., 52, 397
Pont F., Queloz D., Bratschi P, Mayor M., 1997, A&A, 318, 416
Prusti T. et al. (Gaia Collaboration), 2016, A&A, 595, A1
Rastorguev A. S., Dambis A. K., Zabolotskikh M. V., Berdnikov L. N., Gorynya N. A., 2013, in de Grijs R., ed., Advancing the Physics of Cosmic Distances, Proc. IAU Symp. 289, 2012, p. 195
Rastorguev A. S., Utkin N. D., Zabolotskikh M. V., Bajkova A. T., Bobylev V. V., 2017, Astrophys. Bulletin, 72, 122
Reid M. J. et al., 2019, ApJ, 885, 131
Riess A. G. et al., 1998, AJ, 116, 1009
Riess A. et al., 2004, ApJ, 607, 665
Riess A. et al., 2018a, ApJ, 607, 665
Riess A. G. et al., 2018b, preprint (arxiv:1810.03526)
Riess A. G. et al., 2020, preprint (arxiv:2012.08534)
Ripepi V., Molinaro R., Musella I., Marconi M., Leccia S., Eyer L., 2019, A&A, 625, 14
Röser S., Bastian U., 1988, A&AS, 74, 449
Samus' N. N., Kazarovets E. V., Durlevich O. V., Kireeva N. N., Pastukhova E. N., 2017, Astron. Rep., 61, 80
Sandage A., Tammann G. A., 2006, ARA&A, 44, 93
Schmidt B. P. et al., 1998, ApJ, 507, 46
Schönrich R., Binney J., Dehnen W., 2010, MNRAS, 403, 1829
Scolnic D. M. et al., 2018, ApJ, 859, 101
Sedgwick T. M., Collins C. A., Baldry I. K., James P. A., 2021, MNRAS, 500, 3728
Skowron D. M. et al., 2019, Science, 365, 478
Stassun K. G., Torres G., 2018, ApJ, 862, 61
Turner D. G., 2012, J. Amer. Assoc. Variable Star Observers, 40, 502
Udalski A., Kubiak M., Szymański M., 1997, Acta Astron., 47, 319
Vallée J. P., 2017a, Ap&SS, 362, 79
Vallée J. P., 2017b, Astron. Rev., 13, 113
Vallée J. P., 2017c, New Astron. Rev., 79, 49
Vallée J. P., 2018, ApJ, 863, 52
Verde L., Treu T., Riess A. G., 2019, Nature Astron., 3, 891
Wang S., Chen X., 2019, ApJ, 877, 116
Wang S., Chen X., de Grijs R., Deng L., 2018, ApJ, 852, 78
Wegg C., Gerhard O., Portail M., 2015, MNRAS, 450, 4050
Wright E. L. et al., 2010, AJ, 140, 1868
Zabolotskikh M. V., Rastorguev A. S., Dambis A. K., 2002, Astron. Lett., 28, 454
Zinn J. C., Pinsonneault M. H., Huber D., Stello D., 2019, ApJ, 878, 136

This paper has been typeset from a TEX/LATEX file prepared by the author.